Evaluation of 3D Printed Cobalt Iron Cores for Filter Inductors

Jun Wang[1], *Member, IEEE*, Xibo Yuan[1], *Senior Member, IEEE,*
Tuomas Riipinen[2], Jenni Pippuri-Mäkeläinen[2], Sini Metsä-Kortelainen[2] and Tomi Lindroos[2]

[1]Electrical Energy Management Group, University of Bristol, Bristol, BS8 1TR, UK
[2]VTT Technical Research Centre of Finland Ltd, Espoo, 02044, Finland

This paper presents a timely report on 3D printed Cobalt Iron (CoFe) soft magnetic cores enabled by the latest advances of additive manufacturing technologies. The feasibility of 3D printing CoFe magnetic cores is demonstrated in a current-ripple-filtering line inductor for power electronics applications. A like-for-like comparison is conducted between the 3D printed solid core and a commercial laminated core with the identical outer geometries to benchmark the former. Performance of the cores is evaluated based on assembled inductors regarding two key high-frequency characteristics, the inductance and the core losses. The results show that the effective permeability of the 3D printed core reduces rapidly with the increase of frequency, due to the low effective resistivity and consequently prominent eddy currents. When the functional equivalent is achieved, i.e. the same inductance for filtering switching-frequency current ripples, the inductor with 3D printed CoFe cores shows five times larger core losses compared to the commercial laminated core.

***Index Terms*—Additive manufacturing, 3D printing, Cobalt Iron, core loss, inductor, soft magnetic materials**

I. Introduction

Additive manufacturing technologies for power electronics have been actively explored in the past decade [1]. Driven by the trend of developing high-power-density power converters [2] and rapid prototyping, additive manufacturing of electronic components is an attractive option because it enables more flexible and complex shapes and designs, simplified manufacturing process, reduced waste material and faster prototyping cycles.

In power converters, magnetic components, such as inductors and transformers, typically occupy a large portion of the volume/weight and hence require intensive optimization efforts to achieve compact designs. Research has been actively conducted regarding 3D printed magnetic cores [3]–[10]. The materials in these studies are magnetic pastes based on ferrite or powdered iron with the relative permeability ranging from 20 to 70. The typical values of saturation flux density of ferrite and powdered iron are 0.4 T and 1.0 T respectively. Additionally, these studies only focused on toroidal cores.

For high-power applications, gapped filter inductors are widely used. The gapped inductor cores are commonly designed through the Area Product Method [11]–[13], in which the area product is inversely proportional to the maximum allowed flux density B_{pk}. Therefore, by applying a core material with high saturation flux density, more compact inductor designs can be achieved. Compared to ferrite and powdered iron, Cobalt Iron (CoFe) material offers the highest saturation flux density ($B_{max} \approx 2.4$ T) [14]. Additionally, the high thermal conductivity (≈ 30 W/m/K) and high yield strength (≈ 300 MPa) of CoFe also make it an attractive option for applications in harsh environments, such as in aerospace. CoFe material has been used in aerospace industry for high-power-density electric machines [15], [16]. Cobalt Iron laminations are commercially available for fabricating magnetic components, such as the products from Vacuumschmelze®. Previous studies have reported filter inductors built based on laminated CoFe cores [17] for Pulse Width Modulation (PWM) power converters.

Additive manufacturing of CoFe material has been studied recently [18] and has been experimented in the fabrication of electric machine parts. It motivates this work to implement the 3D printed CoFe material into a gapped filter inductor for power electronics applications. Given an existing inductor core made from commercial CoFe laminations [17], this work intends to conduct a like-for-like comparison between a conventional demonstrator and a 3D printed prototype.

This paper aims to provide a timely report on the high-frequency characteristics of world-first 3D printed CoFe inductor cores. The contributions of this work are: (1) demonstration of 3D printing of gapped inductor cores with CoFe material (b) performance evaluation of the 3D printed inductor cores with reference to the commercially available CoFe material. This paper is presented in two parts: (1) manufacturing of the printed core (2) performance evaluation regarding high-frequency inductance and core losses.

II. Additive Manufacturing of Cobalt Iron Cores

To conduct the comparison, the first target is to 3D print a magnetic core as a duplicate of an existing laminated CoFe EE inductor core (presented in [17]) through laser powder-bed fusion (L-PBF). However, it is challenging to 3D print the laminated structure with the current technology, especially the electrical insulations between the laminates. Hence, as a first step, solid soft magnetic cores with the same outer dimensions as the laminated ones are prepared. This section details the manufacturing process.

Firstly, Fe-Co-V powder was produced by gas atomization at VTT Technical Research Centre of Finland Ltd. The chemical composition of the powder as measured with X-Ray Fluorescence Spectrometer (XRF) is listed in Table 1, which matches the common composition of commercial Cobalt Iron alloys [12], [15]. The 2% of vanadium, with appropriate heat-

Manuscript received February 22, 2020; revised April 07, 2020; accepted May 21, 2020. Date of current version May 27, 2020. Corresponding author: Xibo Yuan (email: xibo.yuan@bristol.ac.uk).

Color versions of one or more of the figures in this paper are available online at http://ieeexplore.ieee.org.

Digital Object Identifier (inserted by IEEE).

treatments, improves the ductility but also increases the resistivity of the alloy [19].

TABLE 1 CHEMICAL COMPOSITION OF THE GAS ATOMIZED FE-CO-V POWDER

Si	*S*	*Ti*	*V*	*Cr*	*Mn*	*Fe*	*Co*	*Ni*	*Cu*
0.03	0.02	0.01	2.4	0.22	0.07	49.0	48.2	0.04	0.03

The inductor cores were printed using SLM Solutions GmbH 125HL L-PBF equipped with IPG YLR fiber laser with maximum output of 400 W. An argon atmosphere (99.999% purity) and constant gas flow were maintained in the build chamber for the whole duration of the printing process, where the oxygen level was kept below 0.2%. The following process parameters were used for printing: layer thickness = 30 µm, power = 200 W, scanning speed = 775 mm/s, hatch spacing = 80 µm and scanning strategy with stripe pattern. The inductor cores were printed in vertical orientation on a steel base plate (AISI 314) that was heated to 200 °C. The printed parts were removed from the platform by wire cutting followed by a heat treatment in a pipe furnace in Ar+4%H_2 atmosphere at 820 °C for 10 h, where a heating rate of 200 °C/h and a cooling rate of 100 °C/h were used.

A picture of the printed core and the laminated core is shown in Fig. 1. The 3D printed core successfully replicated the physical dimensions of the existing laminated core.

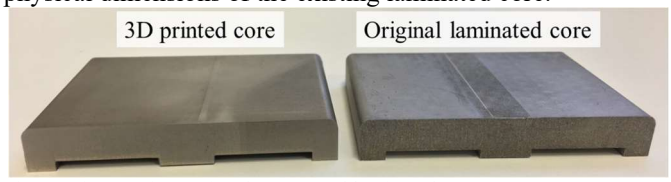

Fig. 1. Picture of 3D printed E core and laminated E core.

A schematic of the designed E core is shown in Fig. 2.

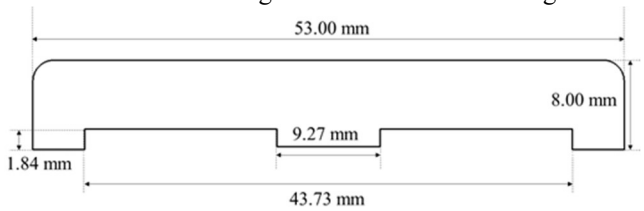

Fig. 2. Schematic of the designed E core (depth = 39.47 mm).

The microstructure of the printed and heat-treated inductor core was examined as it has a significant effect on the magnetic performance. The polished and etched cross-section images of the core are shown in Fig. 3.

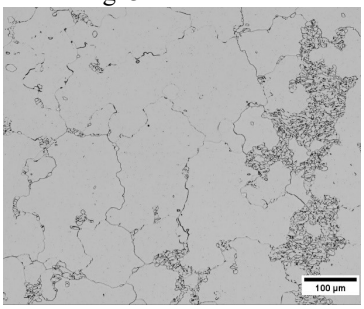

Fig. 3. Cross-section images of polished and etched core after heat treatment.

The printing process produced parts with nearly full density and predominantly large grain size with a small volume of small grains. Similar bimodal grain structure has been reported in an earlier study on L-PBF manufactured CoFe alloys [18], where it was concluded that large grain size resulted in high magnetic permeability and low coercivity. However, as expected, the eddy current losses are high compared to laminated structure, as the printed part is entirely solid allowing large eddy currents to form.

The measured grain size, porosity, resistivity of the 3D printed core and the material density are listed in Table 2. The grain size was measured in accordance with ASTM E112 and ASTM E1181 standards with planimetric method for bimodal grain structure. The porosity was measured from a vertically cut and polished cross-section of a core using ImageJ software (Fiji, GNU license) with measurement area of 259 mm^2. The material density is calculated using the chemical composition.

TABLE 2 PROPERTIES OF THE 3D PRINTED CORES

Grain size	Duplex, Bimodal, 0.8% ASTM No. 13, 99.2%, ASTM No. 3
Porosity	0.01% ± 0.005%
Resistivity	0.435 µΩm
Density	8.24 g/cm^3

III. PERFORMANCE EVALUATION

The performance of the 3D printed CoFe core is evaluated against the reference laminated core in two aspects based on assembled inductors: the inductance and the core losses.

A. Inductance

As the functionality index, the inductances of the assembled inductors are measured with an impedance analyzer, Wayne Kerr 6500B, with a parallel RL model. The original inductor formed by laminated CoFe EE core (shown in Fig. 4) is considered as the baseline for benchmarking.

Fig. 4. Assembled laminated core with number of winding turns $N = 6$.

The measurement results are shown in Table 3.

TABLE 3 MEASURED INDUCTANCE

Frequency	*Set 1 (reference) Commercial laminations (N = 6)* ***LAM-N6***	*Set 2 3D-printed (N = 6)* ***PRINTED-N6***	*Set 3 3D-printed (N = 15)* ***PRINTED-N15***
50 Hz	39.0 µH	29.7 µH	215.6 µH
20 kHz	36.4 µH	3.24 µH	35.3 µH

Comparing *Set 1 (LAM-N6)* and *Set 2 (PRINTED-N6)*, it can be seen that the inductor with 3D printed core can establish 76% inductance of the laminated cores at 50 Hz, with the same core outer geometries and identical windings. The measured relative permeability of the 3D printed CoFe core at 50 Hz can reach 300 ~ 17000 depending on the heat treatment as presented in [18], while the 3D printed inductor core reported in [9] only

offers a relative permeability of 20 ~ 70. The printed inductor cores in this work achieved an effective relative permeability of >10000 at 50 Hz. The effective permeability is extracted from the measured inductance and core geometries as

$$L = \frac{\mu_0 \cdot N^2 \cdot A_c}{\frac{l_m}{\mu_r} + l_g} \quad (1)$$

where μ_0 is the vacuum permeability; N is the number of winding turns; A_c is the effective core cross-section area; l_m is the effective core magnetic path length; μ_r is the relative permeability; l_g is the air gap length; L is the measured inductance.

However, with the increase of frequency, it was found that the 3D printed CoFe core shows a rapid reduction of effective permeability as shown in Fig. 5. With the high-frequency excitation and low effective resistivity, the eddy current phenomenon is prominent in the printed cores. The significant eddy current at higher frequency generates opposing field that subsequently attributes to the decrease of effective permeability and undermines the achieved inductance. Consequently, the established inductance at 20 kHz is only 10% of its low-frequency inductance as shown in Table 3, while the laminated CoFe core still sustains 93% of its nominal value.

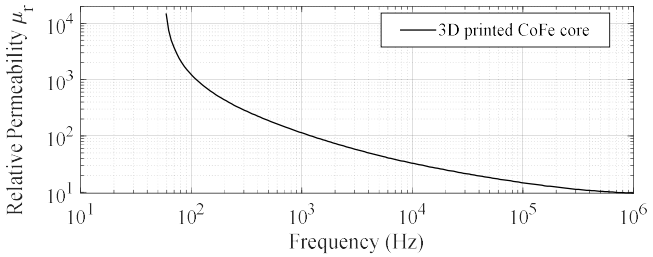

Fig. 5. Extracted effective relative permeability of the 3D printed CoFe core.

The original inductor was designed as a line inductor to filter the switching-frequency current ripples (ΔI filter) to satisfy the allowable current ripple amplitude. The main harmonic component of the triangular current ripples is at around the first and second multiple of the switching frequency [20]. Therefore, to achieve the basic functionality as a ΔI filter inductor, the 3D printed cores must satisfy the target inductance at the range of switching frequency of the power converter, e.g., 20 ~ 100 kHz in this work. With the dimensions of the core fixed, the number of turns N of the 3D printed core is increased from 6 turns to 15 turns (*PRINTED-N15* in Table 3) to compensate the effective permeability reduction and to achieve a comparable inductance as the laminated core at 20 ~ 100 kHz. The measured inductance of the three sets is shown in Fig. 6.

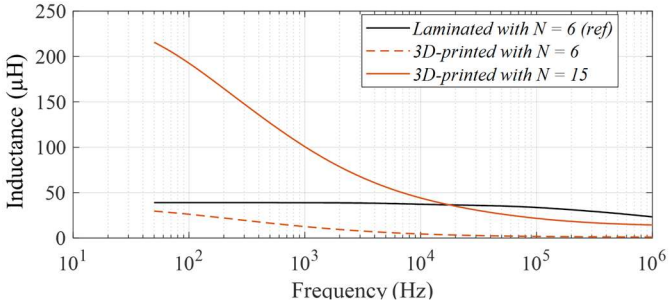

Fig. 6. Measured inductance.

It can be seen that, the *PRINTED-N15* set can reach an inductance level of around 35 μH at 20 kHz, which satisfies the functionality requirement but comes with increased copper loss. A commissioning of the assembled inductors is then conducted with square-wave excitation in the next section.

B. Core Loss Measurement Under Square-wave Excitation

This section focuses on characterizing the high-frequency inductor core losses. From the power electronics design point of view, it is meaningful to compare the core loss of two functional-equivalent inductors, which can achieve the same current ripple in the circuit. Therefore, the following core loss evaluation is performed on the two assembled inductors (*LAM-N6* and *PRINTED-N15*) which have equivalent switching-frequency inductance.

Two-winding dynamic B-H loop measurement has been widely adopted in other studies to measure the inductor core losses [17], [21]–[23] under high-frequency square-wave excitations in power electronics applications. This work also applies this approach to characterize the inductor core losses through the measurement setup illustrated in Fig. 7.

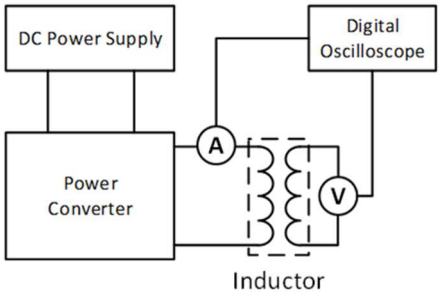

Fig. 7. B-H loop measurement setup.

The principle of this approach is to find the dynamic magnetic field H and flux density B on the inductor core from the measured excitation current I and the open-circuit voltage on the sensing coil U_{L2}, as expressed in (2) and (3).

$$H(t) = \frac{N_1 \cdot I(t)}{l_e} \quad (2)$$

$$B(t) = \frac{1}{N_2 A_e} \int_0^T U_{L2}(t)\, dt \quad (3)$$

where N_1 is the number of turns of the main winding of the inductor; N_2 is the number of turns of the flux-sensing winding; A_e is the effective cross-section area of the core; l_e is the effective length of magnetic path of the core. The total core loss , including hysteresis loss, eddy current loss and residual loss [24], can then be evaluated from the dynamic B-H loop through equation (4) over a period of T.

$$Q = A_e l_e \int H\, dB = \frac{N_1}{N_2} \int_0^T I(t) \cdot U_{L2}(t)\, dt \quad (4)$$

The square-wave excitation voltage is generated by a half-bridge power converter with two DC sources in series that has been presented in [17]. The phase discrepancy between the voltage/current probes are calibrated through a de-skew tool, Keysight U1880A. The inductors are both fitted with 3 turns of secondary sensing windings.

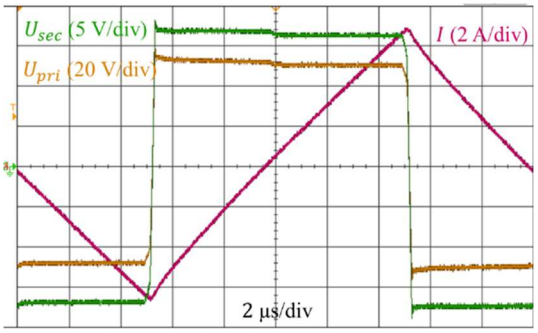

(a) Reference laminated core with $N = 6$ (*LAM-N6*)

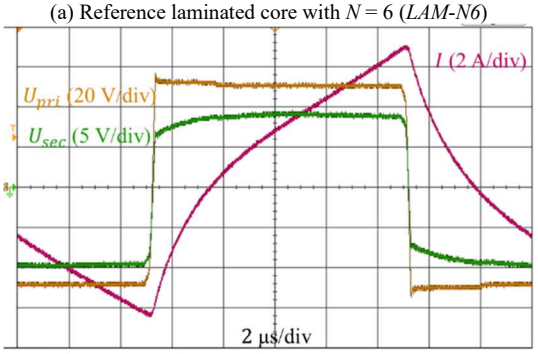

(b) 3D printed core with $N = 15$ (*PRINTED-N15*)

Fig. 8. Current ripple with 50 kHz square-wave excitation.

Fig. 8 shows an example of the excitation voltage and inductor current waveform. It can be seen that the peak-to-peak current ripples in two setups are both approximately 13.4 A, which means the *LAM-N6* and *PRINTED-N15* are equivalent in this case as ΔI filter inductors. It can also be observed that the 3D printed core results in a curvy current response, which indicates a varying inductance, while the laminated core shows a relatively constant inductance and a straight-line current response. The curvy shape of the current is mainly caused by the excessive eddy current. In the printed cores, due to the low effective resistivity, surge eddy currents are induced at the rising/falling edge of excitation voltage, which oppose the rapid change of the excitation magnetic field and subsequently undermines the output inductance. Hence, a steep rise of current can be observed at the rising/falling edge of excitation voltage. Once the eddy currents are decayed later in the cycle, the inductance stabilizes at a higher value and a slower rising rate of the current can be observed.

Corresponding to Fig. 8, *LAM-N6* and *PRINTED-N15* operate in two distinct B-H trajectories as shown in Fig. 9. In these two cases, both the ΔH and ΔB are dissimilar due to the different number of turns N, but the current ripple swings in the circuit are equal as shown in Fig. 8. Mainly due to the excessive eddy currents, *PRINTED-N15* witnesses a wider B-H loop compared to *LAM-N6*. The total core loss indicated by the measured dynamic B-H loops are 2110.6 µJ and 435.9 µJ respectively. To achieve the equivalent current ripple, the core loss in the 3D printed inductor is 4.84 times compared to the laminated core in this case.

A comparison of core loss over various conditions with square-wave excitation is presented in Fig. 10. The inductor core loss profile is generated in the form of a user-friendly loss map proposed in [17], which can be better understood in the context of power electronics. In the user-friendly loss map, the

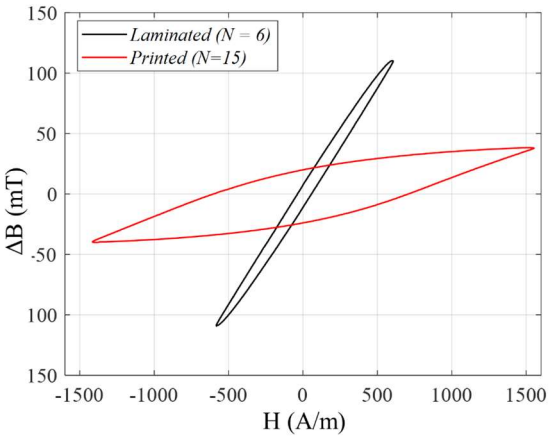

Fig. 9. B-H trajectory of inductor *LAM-N6* and *PRINTED-N15* with equal primary voltage and current ripple (± 6.7 A).

magnetic variables are converted to time-domain electrical variables on the primary side, where U is the amplitude, $U{\cdot}T$ is the volt-time product of the square wave shown in Fig. 8. The pre-magnetization is controlled at zero. Overall, it can be seen that, with the same excitation applied, the 3D printed core shows approximately 5 times the core loss compared to the laminated core, mainly due to the eddy current loss. This is because the 3D printed cores are solid, massive conductors.

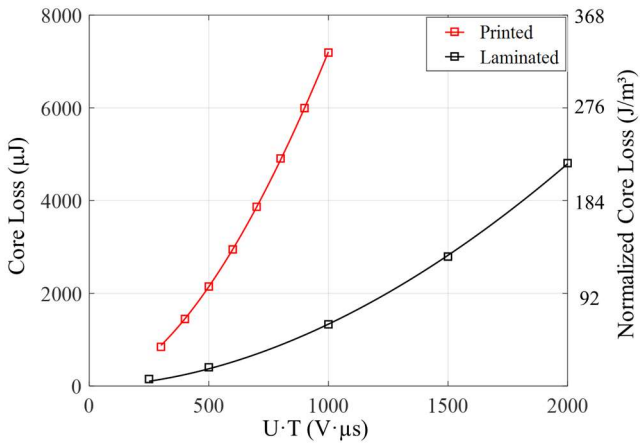

(a) Core Loss vs. $U{\cdot}T$ (V·µs) with $U = 50$ V

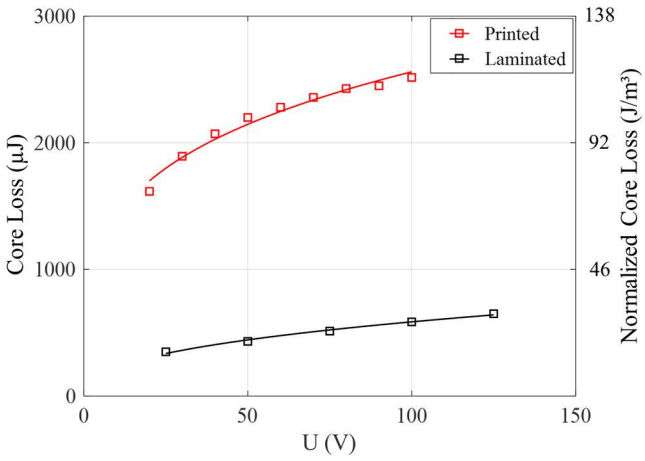

(b) Core Loss vs. U (V) with $U{\cdot}T = 500$ (V·µs)

Fig. 10. Comparison of measured core loss with rectangular excitation.

IV. Conclusion

This work investigated the 3D printed solid CoFe inductor cores with a comparison to conventional laminated cores. It was found that, the effective permeability of the printed solid cores decreases rapidly with increasing frequency because of the prominent eddy current phenomenon. Based on measurements on assembled functional-equivalent inductors, the core losses in the 3D printed cores are considerably higher (e.g. ~5 times) than those in the reference laminated cores with identical outer geometries.

At this stage, the quasi-static DC properties of the 3D printed solid cores already agree with those of commercial counterparts. For the presented high-frequency applications, though the printed component may not yet outperform the conventionally manufactured laminated components, the potential benefits of additive manufacturing, e.g. design freedom, are still attractive and should be constantly explored.

This paper has demonstrated implementing 3D printing of advanced magnetic components in an actual component designed for power electronics applications. It also provides valuable benchmarking results for 3D printed CoFe cores, on which the further work can be built. With the demand of developing high-power-density power converters, the presented technology enables more flexible and complex shapes of the cores to fit in designs with tight spaces. The 3D printing process also enables faster prototyping cycles.

Loss mitigation is one of the key directions for future improvements. Through geometrical modifications presented in [25], the electric resistivity of 3D printed soft magnetic cores can be increased from 0.435 μΩm to 0.587 μΩm. Consequently, the core losses can be reduced at least by 50% in this case. With the undergoing development for further performance improvement, the studied technology presents a potential for high-frequency power electronics applications. Furthermore, to exploit the benefits of 3D printed components, the inductor design and optimization will be revisited in the future to find the possible performance gains against the state-of-the-art 2D manufacturing methods.

Acknowledgment

Jenni Pippuri-Mäkeläinen would like to thank the Academy of Finland for funding this work in part under decision number 289338.

References

[1] Y. Xu and C. Deng, "An investigation on 3D printing technology for power electronic converters," in *IEEE Proc. Int. Symposium on Power Electronics for Distributed Generation Systems*, 2017.

[2] J. W. Kolar *et al.*, "PWM Converter Power Density Barriers," *IEEJ Transactions on Industry Applications*, vol. 128, no. 4, pp. 468–480, 2012.

[3] L. Liu *et al.*, "Design and additive manufacturing of multi-permeability magnetic cores," in *IEEE Proc. Energy Conversion Congress and Exposition*, 2017.

[4] C. Ding, L. Liu, Y. Mei, K. D. T. Ngo, and G. Q. Lu, "Magnetic paste as feedstock for additive manufacturing of power magnetics," in *IEEE Proc. Applied Power Electronics Conference and Exposition*, 2018.

[5] C. Ding, L. Liu, J. Moss, J. Mullenix, K. D. T. Ngo, and G.-Q. Lu, "Reliability assessment of 3D-printed pot-core constant-flux inductors," in *IEEE Proc. Energy Conversion Congress and Exposition*, 2018.

[6] D. Bowen and D. Basu, "Exploration of the 3-D printing of transformer structures with embedded ferrite cores," *IEEE Transactions on Magnetics*, vol. 55, no. 2, Feb. 2019.

[7] S. Lu, C. Ding, Y. Mei, K. D. T. Ngo, and G.-Q. Lu, "Hetero-magnetic coupled inductor (HMCI) for high frequency interleaved multiphase DC/DC converters," in *IEEE Proc. Applied Power Electronics Conference and Exposition*, 2019.

[8] L. Liu, T. Ge, Y. Yan, K. D. T. Ngo, and G. Q. Lu, "UV-assisted 3D-printing of soft ferrite magnetic components for power electronics integration," in *Int. Conf. on Electronics Packaging*, 2017.

[9] Y. Yan, J. Moss, K. D. T. Ngo, Y. Mei, and G. Q. Lu, "Additive Manufacturing of Toroid Inductor for Power Electronics Applications," *IEEE Transactions on Industry Applications*, vol. 53, no. 6, pp. 5709–5714, 2017.

[10] L. Liu *et al.*, "Design and additive manufacturing of multipermeability magnetic cores," *IEEE Transactions on Industry Applications*, vol. 54, no. 4, pp. 3541–3547, 2018.

[11] N. Mohan, T. M. Undeland, and W. P. Robbins, *Power Electronics - Converters, Applications, and Design 3rd Edition*. WILEY, 2003.

[12] Colonel Wm. T. McLyman, *Transformer and Inductor Design Handbook*, 4th ed. Boca Raton: CRC Press, 2011.

[13] K. K. Marian, *High-Frequency Magnetic Components*, 2nd ed. Chichester: WILEY, 2014.

[14] R. V. Major and C. M. Orrock, "High saturation ternary cobalt-iron basalt alloys," *IEEE Transactions on Magnetics*, vol. 24, no. 2, pp. 1856–1858, Mar. 1988.

[15] M. Cossale, A. Krings, J. Soulard, A. Boglietti, and A. Cavagnino, "Practical investigations on cobalt-iron laminations for electrical machines," *IEEE Transactions on Industry Applications*, vol. 51, no. 4, pp. 2933–2939, 2015.

[16] N. Simpson, T. Duggan, P. H. Mellor, and J. D. Booker, "Measurement of the thermal characteristics of a stator-housing interface," in *Proc. IEEE International Symposium on Diagnostics for Electrical Machines, Power Electronics and Drives (SDEMPED)*, 2017, pp. 557–564.

[17] J. Wang, K. J. Dagan, X. Yuan, W. Wang, and P. H. Mellor, "A practical approach for core loss estimation of a high-current gapped inductor in PWM converters with a user-friendly loss map," *IEEE Transactions on Power Electronics*, vol. 34, no. 6, pp. 5697–5710, Jun. 2019.

[18] T. Riipinen, S. Metsä-Kortelainen, T. Lindroos, J. Keränen, A. Manninen, and J. Pippuri-Mäkeläinen, "Properties of soft magnetic Fe-Co-V alloy produced by laser powder bed fusion," *Rapid Prototyping Journal*, vol. 25, no. 4, 2018.

[19] R. S. Sundar and S. C. Deevi, "Soft magnetic FeCo alloys: alloy development, processing, and properties," *International Materials Reviews*, vol. 50, no. 3, pp. 157–192, Jul. 2005.

[20] D. G. Holmes and T. A. Lipo, *Pulse Width Modulation for Power Converters*. WILEY, 2003.

[21] V. J. Thottuvelil, T. G. Wilson, and H. A. Owen, "High-frequency measurement techniques for magnetic cores," *IEEE Transactions on Power Electronics*, vol. 5, no. 1, pp. 41–53, 1990.

[22] F. D. Tan, J. L. Vollin, and S. M. Cuk, "A practical approach for magnetic core-loss characterization," *IEEE Transactions on Power Electronics*, vol. 10, no. 2, pp. 572–578, Mar. 1995.

[23] T. Shimizu and S. Iyasu, "A practical iron loss calculation for AC filter inductors used in PWM inverters," *IEEE Transactions on Industrial Electronics*, vol. 56, no. 7, pp. 2600–2609, 2009.

[24] S. Iyasu, T. Shimizu, and K. Ishii, "A novel inductor loss calculation method on power converters based on dynamic minor loop," *IEEJ Transactions on Industry Applications*, vol. 126, no. 7, pp. 1028–1034, 2006.

[25] T. Riipinen, J. Pippuri-Mäkeläinen, T. Lindroos, S. Metsä-Kortelainen, J. Keränen, and A. Manninen, "Topology optimized soft magnetic cores by laser powder bed fusion," in *Conf. Europe Powder Metallurgy Congress and Exhibition*, 2019.